*energies*

MDPI

*Article*

# Multiobjective Optimization of Cement-Based Panels Enhanced with Microencapsulated Phase Change Materials for Building Energy Applications

**Facundo Bre [1,2,*], Antonio Caggiano [3] and Eduardus A. B. Koenders [1]**

[1] Institut für Werkstoffe im Bauwesen, Technische Universität Darmstadt, 64287 Darmstadt, Germany; koenders@wib.tu-darmstadt.de
[2] Centro de Investigación de Métodos Computacionales (CIMEC), UNL, CONICET, Predio "Dr. Alberto Cassano", Colectora Ruta Nacional 168, Paraje El Pozo, Santa Fe 3000, Argentina; facubre@cimec.santafe-conicet.gov.ar
[3] DICCA, Department of Civil, Chemical and Environmental Engineering, University of Genova, Via Montallegro 1, 16145 Genova, Italy; antonio.caggiano@unige.it
* Correspondence: bre@wib.tu-darmstadt.de or facubre@cimec.santafe-conicet.gov.ar

**Abstract:** Thermal energy storage using phase change materials (PCMs) is a promising technology for improving the thermal performance of buildings and reducing their energy consumption. However, the effectiveness of passive PCMs in buildings depends on their optimal design regarding the building typology and typical climate conditions. Within this context, the present contribution introduces a novel multiobjective computational method to optimize the thermophysical properties of cementitious building panels enhanced with a microencapsulated PCM (MPCM). To achieve this, a parametric model for PCM-based cementitious composites is developed in EnergyPlus, considering as design variables the melting temperature of PCMs and the thickness and thermal conductivity of the panel. A multiobjective genetic algorithm is dynamically coupled with the building energy model to find the best trade-off between annual heating and cooling loads. The optimization results obtained for a case study building in Sofia (Bulgaria-EU) reveal that the annual heating and cooling loads have contradictory performances regarding the thermophysical properties studied. A thick MPCM-enhanced panel with a melting temperature of 22 °C is needed to reduce the heating loads, while a thin panel with a melting temperature of 27 °C is required to mitigate the cooling loads. Using these designs, the annual heating and cooling loads decrease by 23% and 3%, respectively. Moreover, up to 12.4% cooling load reduction is reached if the thermal conductivity of the panels is increased. Therefore, it is also concluded that the thermal conductivity of the cement-based panels can significantly influence the effectiveness of MPCMs in buildings.

**Keywords:** phase change material; cement-based panels; thermophysical properties; energy-efficient buildings; multiobjective optimization; building performance simulation



**Citation:** Bre, F.; Caggiano, F.; Koenders, E.A.B. Multiobjective Optimization of Cement-Based Panels Enhanced with Microencapsulated Phase Change Materials for Building Energy Applications. *Energies* **2022**, *15*, 5192. https://doi.org/10.3390/en15145192

Academic Editors: Przemysław Brzyski and Alessandro Cannavale

Received: 23 June 2022
Accepted: 15 July 2022
Published: 18 July 2022

**Publisher's Note:** MDPI stays neutral with regard to jurisdictional claims in published maps and institutional affiliations.



## 1. Introduction

The design of energy-efficient buildings has become a major global challenge for both science and industry. This is mainly driven by the urgent need to significantly reduce the emission of gases that provoke the greenhouse effect and climate change [1]. The building stock handles over one-third of the global energy consumption, and with this, nearly 40% of total direct and indirect $CO_2$ emissions. This sector also remains the single largest energy consumer in the European Union [2].

Among the existing technologies for improving building energy efficiency, innovative thermal energy storage (TES) systems have shown great potential for saving energy [3]. Particularly, TES technologies based on latent heat, such as those using phase change materials (PCMs), have attracted significant attention from the construction sector in the

last few decades. This interest is because of their high energy storage density; i.e., large amounts of heat energy can be stored in small PCM volumes [4].

PCMs undergo a phase transition (solid–liquid or liquid–solid) around their utilization temperature, through which they can store (during melting) and release (during solidification) large amounts of heat energy. For most PCMs, this transition is achieved at an almost constant temperature, which is commonly referred to as the melting temperature. Exploiting this physical phenomenon, PCMs can be incorporated into building components to increase their heat storage capacity and achieve a stabilizing thermal effect in indoor spaces [5].

Thus, by employing PCMs in buildings, it is possible to reduce the energy demand, mitigate peak heating and cooling loads, and improve indoor thermal comfort. PCMs can be actively employed in various ways, such as being integrated into mechanical ventilation systems, embedded in active cooling/heating systems for water or other fluids, and/or encapsulated in pipe networks [6]. PCMs can also be used passively by integrating them into building components, for example, by direct incorporation, immersion, encapsulation, microencapsulation, and shape-stabilization [7].

Despite its enormous energy-saving potential, the successful use of passive PCM-based systems in buildings is not implicitly guaranteed. This is because the PCM performance strongly depends on the interplay between the daily thermal cycles. If PCMs are not accurately designed for a specific application, they may not have sufficient benefits or, even worse, they may generate undesired thermal effects. To achieve the accurate performance of PCMs in buildings, a proper design of their thermophysical properties, their quantities, and their positions is required [8,9]. However, this is highly influenced by the building typology and local climate conditions, suggesting the use of advanced design methods such as building performance simulation (BPS) software [10]. These tools are essential for achieving energy-efficient building designs in real climate conditions [11].

A drawback also present in PCMs is their low thermal conductivity, which often can compromise their proper activation (i.e., solidification/melting). In this regard, plenty of heat transfer enhancements have been proposed in the literature to improve the energy storage/release of latent-based systems such as those which employ PCM-based composites. They are often based on either play/design with the tune geometry of the device or system for TES usage [12] or to increase the thermal conductivity of the PCM-based composite. The latter can be achieved by using additions and/or high-conducting particles such as carbon microfibers [13,14], fine materials such as copper [15], graphite [16], aluminum [17], bronze [18], nickel and stainless steel [19], graphene nano-platelets [20], and carbon nanotubes [21].

Regarding the available models to predict the performance of building enclosures with PCMs, there are several approaches of different levels of complexity: simplified, intermediate, and sophisticated models [22]. However, most of the PCM models integrated into whole-building simulation programs correspond to those classified as intermediate models, which are based on the heat source method, the heat capacity method, and the enthalpy method. Among them, the effective heat capacity method and the heat source method are implemented in ESP-r [23]. Several PCM models have been developed in TRNSYS, including also the heat capacity (e.g., "TYPE260") and the heat source methods (e.g., "TYPE1270") [22]. Finally, the enthalpy method, which is the most complex one among the intermediate options, is the PCM model implemented in EnergyPlus software [24].

In the current literature, several studies aim to address the optimization of the PCMs' thermophysical properties for building applications. Using a parametric analysis, Ascione et al. [25] studied the proper position and melting temperature of a PCM to achieve nearly zero-energy buildings in Mediterranean climates. They concluded that using a PCM melting temperature of 25 °C on the inner side is recommended, and this can achieve reductions in cooling energy demand from 2% (in Madrid) to 13% (in Naples). Saffari et al. [9] performed a simulation-based optimization analysis of PCM melting temperature to improve the energy performance in buildings across different climate regions regarding the Köppen–Geiger classification. By applying this method, they demonstrated that the optimal selection of

the PCM melting temperature can highly influence the total energy consumption of a building, and this strongly depends on the considered climatic conditions. The results also showed that an increment in the PCM quantity can both increase and decrease the performance of the PCMs significantly, affecting their benefits. Therefore, although this work presented significant developments, in some cases, no clear relationships between the PCM thermophysical properties and the heating/cooling energy savings could be derived. This arises from the fact that the research was carried out by employing a single objective optimization approach. Recently, Arıcı et al. [26] carried out an optimization study about the maximum activation of latent heat of PCM integrated into external building walls for three cities in Turkey. In this work, the influence of location, melting temperature, and layer thickness of PCM on building energy saving was evaluated. However, the PCM design was addressed by adopting a single-objective optimization approach. In addition, the thermal performance of the building was characterized by a single wall heat balance instead of one involving the whole building. This hypothesis can induce non-physical conclusions about the optimal position of the PCM and its melting temperature. For cementitious materials enhanced with microencapsulated PCM (MPCM), most of the current efforts are focused on the development of the materials only and do not evaluate the performance of this technology integrated into buildings regarding real climate conditions [27–29].

To address the pinpointed limitations, this work proposes a novel method based on multiobjective optimization to design cement-based systems for building applications enhanced with PCM. In particular, the method is devoted to finding the optimal thermophysical properties of cement-based building panels with embedded MPCM and following annual heating/cooling loads. The PCM melting temperature and the thickness and thermal conductivity of the cement-based panel are the design variables. Thus, this new approach provides a general method to explore the relationship between optimal thermophysical properties of PCM-based systems and the heating/cooling performance of the building incorporating them. This allows for important contributions to a better understanding of the real performance of passive PCM-based systems in buildings.

## 2. Methods

### *2.1. Case Study Building*

The ANSI/ASHRAE Standard 140-2011 BESTEST 9001 [30] is employed to evaluate the thermal performance of the different PCM-based cementitious panels. This baseline model is a rectangular single zone (8 m wide × 6 m long × 2.7 m high) with no interior partitions and 12 $m^2$ of windows on the South exposure; see Figure 1. A power of 200 W (60% radiative and 40% convective) is set as the internal load, and a highly insulated slab is employed to minimize the thermal coupling between the ground and indoors. The construction characteristics of the walls are detailed in Table 1.

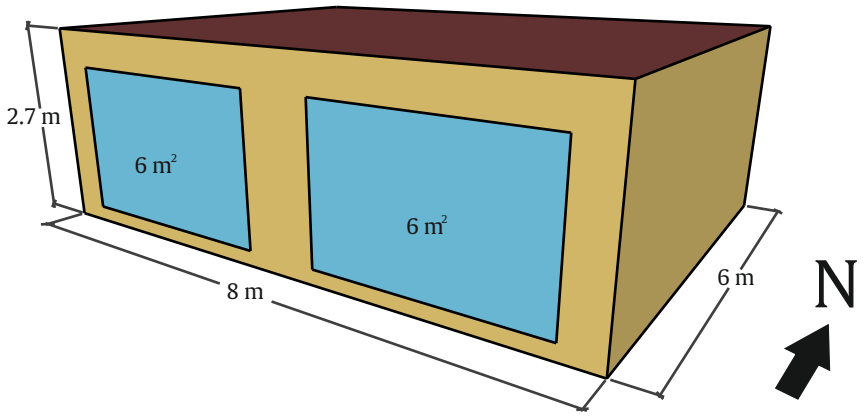


**Figure 1.** Isometric view of the baseline building employed (BESTEST 900).

**Table 1.** Wall characteristics of the BESTEST 900 [31].

| Element | k (W/(m·K)) | Thickness (m) | U (W/(K·m$^2$)) | R ((K·m$^2$)/W) | Density (kg/m$^3$) | $c_p$ (Sensible) (J/(kg·K)) |
|---|---|---|---|---|---|---|
| Int. Surface Coeff. | | | 8.290 | 0.121 | | |
| Concrete Block | 0.51 | 0.1000 | 5.100 | 0.196 | 1400 | 1000 |
| Foam Insulation | 0.04 | 0.0615 | 0.651 | 1.537 | 10 | 1400 |
| Wood Siding | 0.14 | 0.0090 | 15.556 | 0.064 | 530 | 900 |
| Ext. Surface Coeff. | | | 29.300 | 0.034 | | |
| Overall, air-to-air | | | 0.512 | 1.952 | | |

Following the setting described in the ANSI/ASHRAE Standard 140-2011 [30], the energy model of the BESTEST 900 is implemented in the software EnergyPlus [32]—version 9.5 [33].

The building is assumed in Sofia (Bulgaria-EU), where three BESTEST 900 are currently under construction to full scale. These prototypes will be employed to experimentally measure the performance of several NRG-FOAMs developed within the NRG-STORAGE project [34]. The climate in Sofia is classified as a 5A zone (Cool—Humid) according to the ASHRAE 169-2013 [35] and as a CFB region according to the Köppen–Geiger Climate Classification [36].

To characterize the energy performance of the building, the BESTEST 900 employs an ideal HVAC system whose thermostat control is set to 20 °C for heating and 27 °C for cooling. Thus, the performance of each candidate design is evaluated by the ideal annual loads for heating and cooling. These are calculated for the recent typical meteorological year (TMYx.2004-2018) in Sofia, which is taken from [37].

### *2.2. PCM-Based Cementitious Composite Design and Modeling*

Figure 2 shows the wall material configuration considered. A cement-based layer enhanced with MPCM is added to the inside of the existing walls. The thermophysical properties of this cement-based layer are taken from the experimental results obtained by Mankel et al. [38]. In that study, nine mixtures, made of three different water/cement (w/c) ratios and various amounts of MPCM volume fractions, were considered. The MPCM employed was powder-like microencapsulation filled with a commercial paraffin wax, Micronal® DS 5038 X by BASF [39]. For this work, the mixture with w/c = 0.4 and 20% of MPCM volume fraction is employed. Table 2 shows the thermophysical properties of the chosen material. The melting temperature of the PCM is characterized using the peak melting temperature ($T_{peak}$), which is defined as the temperature where the PCM reaches the maximum thermal capacity.

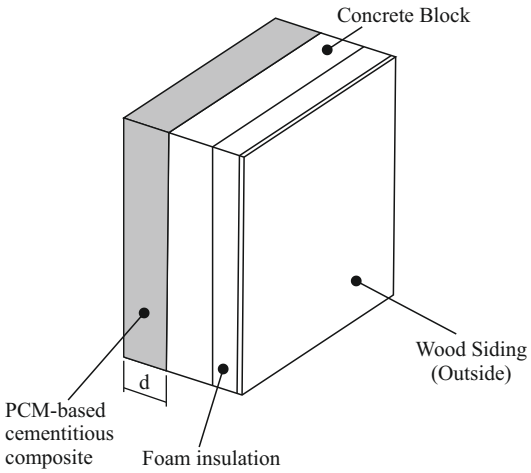


**Figure 2.** Wall material configuration.

The latent thermal capacity of the panel is represented by using the PCM model (Material Property: Phase Change) of EnergyPlus, which has been widely validated against different analytical solutions and experimental results [40–42]. Moreover, this model is

based on the enthalpy ($h$) approach that also was previously validated by the authors of this paper [43,44]. Thus, this model employs the $h - T$ curve to iteratively compute the specific thermal capacity property of the materials, at each time step, as:

$$c_p(T) = \frac{h_i^j - h_i^{j-1}}{T_i^j - T_i^{j-1}}, \quad (1)$$

where $h$ is the enthalpy (J/kg), $T$ is the temperature (°C), $i$ indicates the node, and $j$ and $j-1$ indicate the current and previous time steps, respectively. To simulate PCM in EnergyPlus, the conduction finite difference (*CondFD*) solution algorithm is employed along with 30 time-steps per hour to guarantee accurate results [40].

**Table 2.** Thermophysical properties of the MPCM-based cementitious composite [38].

| Thermophysical Property | Value |
|---|---|
| $c_p$ (sensible) | 938 J/(kg·K) |
| k | 0.473 W/(m·K) |
| Density | 1671.7 kg/m$^3$ |
| $T_{peak}$ | 24.5 °C |

The latent thermal capacity values of the MPCM-based cementitious composite (i.e., $c_p - T$ and $h - T$ curves) are depicted in Figure 3a,b, respectively. Regarding the enthalpy curve, the original one has a $T_{peak}$ of 24.5 °C (see the green central curve in Figure 3b). It is worth noting that this is the melting curve of the material, while the hysteresis of the PCM is not considered, because still, there are no reliable models to represent this phenomenon [45,46]. To study the optimal design of the PCM properties, a shift range of +10/−10 °C is numerically allowed for the $T_{peak}$, as also shown in Figure 3b.

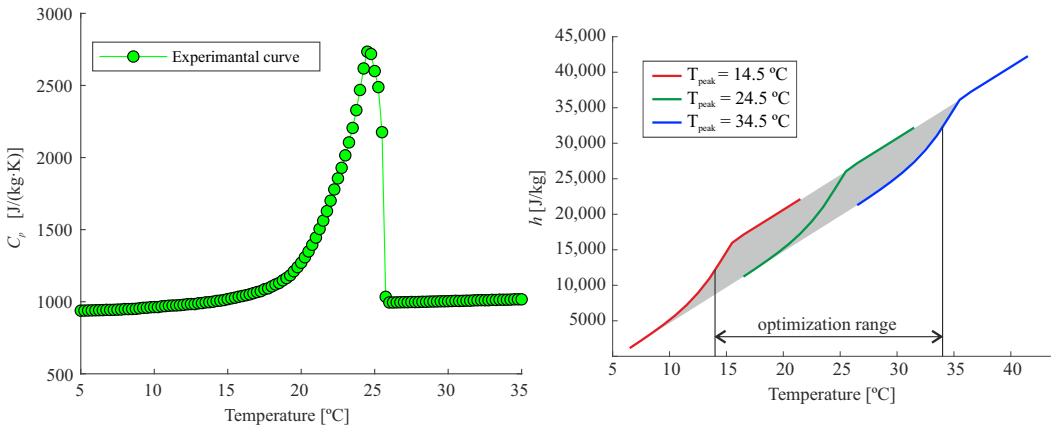


**Figure 3.** MPCM-based cementitious composite: (**a**) Experimental $c_p - T$ curve obtained in [38]; (**b**) Enthalpy curve model and the shift range allowed for the $T_{peak}$.

Table 3 summarizes the details of the building configuration and the PCM model used in EnergyPlus. The setup of the algorithms is based on the guidelines described in [31]. For further details about the building energy model, see ANSI/ASHRAE Standard 140-2011 (cf. Section 5.2.1). This information is also able to be found in the EnergyPlus input files (IDF), which are provided as supplementary research data of this article.

**Table 3.** Details of the building model configuration used in EnergyPlus for the BESTEST 900.

| Model | Details | Setting |
|---|---|---|
| General configurations | North axis | 0 |
| | Site:Location | Sofia (Bulgaria-EU) |
| | Terrain | Suburbs |
| | Solar distribution | FullInteriorAndExterior |
| | SurfaceConvectionAlgorithm: Inside | TARP |
| | SurfaceConvectionAlgorithm: Outside | DOE-2 |
| External wall | U-factor (no film) (W/(K·m$^2$)) | 0.556 |
| | External solar absorptance (0–1) | 0.6 |
| | Internal solar absorptance (0–1) | 0.6 |
| Roof | U-factor (no film) (W/(K·m$^2$)) | 0.334 |
| | External solar absorptance (0–1) | 0.6 |
| | Internal solar absorptance (0–1) | 0.6 |
| Floor | U-factor (no film) (W/(K·m$^2$)) | 0.04 |
| | External solar absorptance (0–1) | 0.6 |
| | Internal solar absorptance (0–1) | 0.6 |
| Window | U-factor (no film) (W/(K·m$^2$)) | 2.721 |
| | Visible tramitance (0–1) | 0.767 |
| | Glass type | Double Pane |
| | Window to wall ratio | 0.55 |
| Geometry | Number of floors | 1 |
| | Height (m) | 2.7 |
| | Total conditioned area of floors (m$^2$) | 48 |
| Internal gains | Equipments: Design Level (W) | 200 |
| | Equipments: Fraction Radiant | 0.6 |
| Ventilation | Type modeling | Infiltration |
| | Infiltration rate (ACH) | 0.5 |
| AC system | Type | Ideals loads |
| | Heating setpoint (°C) | 20 |
| | Cooling setpoint (°C) | 27 |
| | Dehumidification | No |
| | Outdoor Air Flow Rate per Person (m$^3$/s) | 0.00944 |
| PCM model | MaterialProperty:PhaseChange | Enthalpy curve |
| | HeatBalanceAlgorithm | ConductionFiniteDifference |
| | Timesteps | 30 |

### *2.3. Multiobjective Optimization Approach*

In the presence of mutually conflicting objectives, the solution of the architectural design of an energy-efficient building is not unique but rather a set of non-dominated solutions [47]. This set is commonly referred to as the Pareto front because of the dominance concept introduced by Pareto [48]. A solution is defined as non-dominated (i.e., Pareto-optimal) whether there is not any other feasible solution that improves one objective without deteriorating at least one another. This concept is also present in the optimization of PCMs in buildings, since the heating and cooling energy were shown to be mutually contradictory regarding some PCM design parameters, such as the PCM melting temperatures and the PCM quantities [5,8,9]. Thus, a multiobjective optimization approach is proposed to find the optimal set of parameters defining the PCM-based cementitious panel that improves the energy performance of the building. This can be mathematically described by the following bi-objective optimization problem:

$$\begin{aligned} &\min_{\mathbf{x}\in\mathcal{V}} && [f_1(\mathbf{x}), f_2(\mathbf{x})] \\ &\text{subject to :} && \\ & && x_i^L \leq x_i \leq x_i^U,\ i = 1, \ldots, n; \end{aligned} \tag{2}$$

where $x_i^L$ and $x_i^U$ are the lower and upper limits for the corresponding design variable $x_i$; see Table 4 in Section 2.4. The objectives $f_1(\mathbf{x})$ and $f_2(\mathbf{x})$ are the annual heating and cooling ideal loads of the building, respectively. These are obtained as a result of the EnergyPlus simulations for each candidate design evaluated during the optimization process.

To solve the unconstrained optimization problem (2), the multiobjective Non-dominated Sorting Genetic Algorithm-II (NSGA-II) [49] is dynamically coupled with the EnergyPlus software [32]. Several truly multiobjective optimization solvers have been tested to solve building energy optimization problems such as the (2) [50], for instance, SPA2 [51], MOPSO [52], and NSGA-II [49]. These evolutionary algorithms are well suited for parallel computing, do not "get stuck" in local optima, and have low sensitivity to discontinuities in the objective functions, which make them the preferred solvers for addressing building energy optimization problems [53]. The choice of NSGA-II for this research is because it stands out from others due to several desired features, such as the efficient sorting of non-dominated solutions, accounting for elitism (which speeds up the convergence) and the wide diversity of optimal solutions obtained along the Pareto front. This latter capability is relevant in the current study to observe the relationship between the optimal thermophysical properties of the MPCM-based panels and the energy performance of the buildings that use these panels. The capability of NSGA-II to obtain a set of optimal solutions well-distributed along the Pareto front was validated in our previous works [47,54].

Figure 4 shows the general workflow of the optimization method proposed in this work. Thus, during the optimization process, at each fitness step, the objective functions are computed for each individual in the population via an EnergyPlus simulation. This means that the PCM model of each EnergyPlus simulation is dynamically set according to the design variables proposed by the optimization algorithm. This procedure continues until it reaches the stopping criterion. The optimization method proposed is implemented on the Distributed Evolutionary Algorithms in Python (DEAP) [55] platform. For further details on this implementation, see [54].

### *2.4. Optimization Case Studies*

From the basic cementitious panel enhanced with MPCM, two optimization problems are formulated according to the considered design variables. In the first one, Case A, the optimization variables are the thickness of the panel (d) and the $T_{peak}$ of the PCM. In the second one, Case B, the thermal conductivity of the panel is also simultaneously optimized along with the design variables of Case A to achieve a deeper understanding of the relationship between this property and the effectiveness of PCMs. Table 4 summarizes the design variables and the optimization ranges that are considered for the two case studies.

**Table 4.** Design variables and their ranges for the case studies.

| Design Variable | Case A | | Case B | |
|---|---|---|---|---|
| | $x^L$ | $x^U$ | $x^L$ | $x^U$ |
| d (m) | 0.05 | 0.35 | 0.05 | 0.35 |
| $T_{peak}$ (°C) | 14.5 | 34.5 | 14.5 | 34.5 |
| k (W/(m·K)) | - | - | 0.47 | 10.0 |

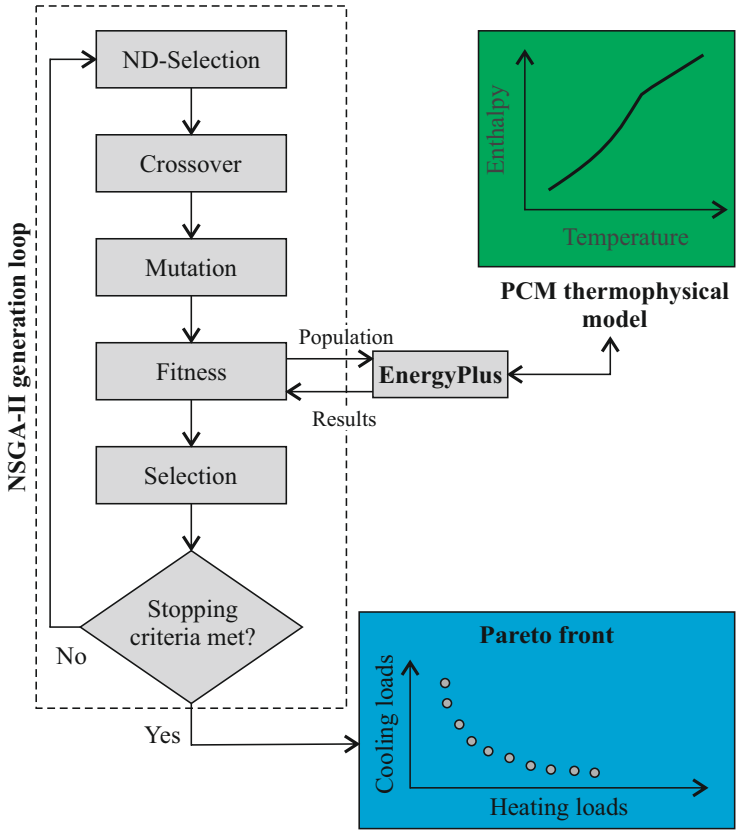


**Figure 4.** Schematic workflow of the proposed method.

The NSGA-II settings for solving the optimization problems in each case study, Case A and Case B, are detailed in Table 5. So, 4800 EnergyPlus simulations are solved in each optimization problem by using a population size of 48 individuals and 100 generations.

**Table 5.** Settings of the NSGA-II for the optimization case studies.

| Item | Value |
|---|---|
| Population size | 48 |
| Number of generations | 100 |
| Selection | Tournament |
| Crossover method | Blended method |
| Crossover probability | 90% |
| Mutation method | Gaussian |
| Mutation probability | 0.2% |

## 3. Results

This section reports the analysis and discussion of the optimization results obtained for the proposed case studies. First, the optimization results for Case A are analyzed in Section 3.1. Then, the corresponding results for Case B are presented in Section 3.2. Finally, a comparative discussion between both case studies is performed in Section 3.3. For closer analysis (or their reproduction), all the optimization results are provided as supplementary research data.

### *3.1. Optimization of Case A*

Figure 5 shows the multiobjective optimization results of the annual ideal loads for heating and cooling obtained for Case A. These include the best trade-off (Pareto front) between heating and cooling loads and all the feasible designs evaluated during the optimization procedure. The heating and cooling loads of the baseline model are also displayed to obtain a reference of the improvements reached by the optimized designs.

The first observation is that a reduction in both heating and cooling loads can be obtained by including the PCM-based panel in the building. Moreover, the best performance of the building for heating and cooling has a mutually contradictory response regarding the optimum design of the PCM melting temperature (i.e., $T_{peak}$ of melting) and the thickness of the panel (d). This means that the best solution for heating is not the best design for cooling and vice versa. This is an important conclusion that demonstrates the necessity of using a multiobjective approach to design passive PCM-based systems in building applications.

Regarding the optimized designs (Pareto front), Figure 5 also highlights that most of them simultaneously improve the heating and cooling performance compared to the baseline model. Only a few designs show a slightly lower performance for cooling than the baseline model.

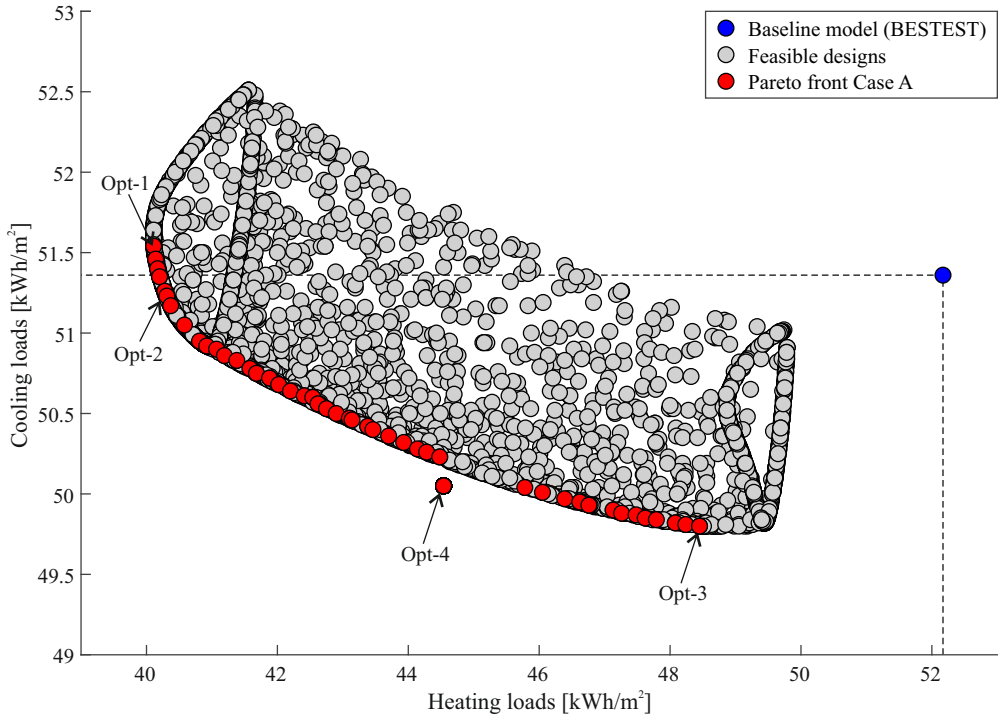


**Figure 5.** Optimization results of the annual ideal loads for heating and cooling obtained for Case A.

Table 6 summarizes the performance of the different optimal designs obtained (Opt-1 to Opt-3) and their relative improvements compared to the baseline model. Regarding the best design for heating (Opt-1), this achieves a large saving of 23.12% for heating, while its cooling performance slightly worsens (−0.35%). Opt-3 is the best design for cooling, which reduces 3.04% of cooling loads and 7.13% of the heating loads. Finally, Opt-2 is the design with the minimum total loads (heating + cooling), achieving a reduction of 11.58%, with improvements of 22.73% and 0.25% for heating and cooling, respectively. From this quantitative analysis, it is noted that all the optimized designs can easier improve the heating performance than the cooling one. Even in the best design for cooling, only an improvement of 3.04% could be achieved, while heating loads can be reduced by 7.13% compared to the baseline model.

**Table 6.** Performances of the optimized designs for Case A. The best design for each case is in bold.

| | Heating Loads (kWh/m$^2$) | Cooling Loads (kWh/m$^2$) | Total Loads (kWh/m$^2$) | Heating Saving (%) | Cooling Saving (%) | Total Saving (%) |
|---|---|---|---|---|---|---|
| Baseline | 52.17 | 51.36 | 103.53 | - | - | - |
| Opt-1 | 40.11 | 51.54 | 91.65 | **23.12** | −0.35 | 11.47 |
| Opt-2 | 40.31 | 51.23 | 91.54 | 22.73 | 0.25 | **11.58** |
| Opt-3 | 48.45 | 49.80 | 98.25 | 7.13 | **3.04** | 5.10 |

Figure 6 shows the relationship between the design variables of all the optimal results (Pareto front) obtained in Case A. This analysis enables a better understanding of the relationship between the optimum design variables and the energy performance of the building. Therefore, it can be seen that the best building performance for heating (Opt-1) is achieved for the thickest panel analyzed (0.35 m) and a $T_{peak}$ = 22.31 °C. Conversely, the best performance for cooling (Opt-3) is reached by using a thin panel of 0.073 m and a $T_{peak}$ = 27.26 °C. Moreover, the design that minimizes the total loads (Opt-2) also employs the thickest panel analyzed (0.35 m) but along with a $T_{peak}$ = 23.98 °C.

Despite a wide range of PCM melting temperatures that are numerically being analyzed, except for Opt-4, the optimum designs are found with $T_{peak}$ laying between 22.31 and 27.26 °C. The physical reason for this range of optimum melting temperature is that the latent heat storage in PCMs with higher or lower $T_{peak}$ does not considerably affect the heating and cooling loads that are evaluated in the indoor air. Opt-4 is an atypical design defined by the thickest panel (0.35 m) and a $T_{peak}$ = 29.26 °C.

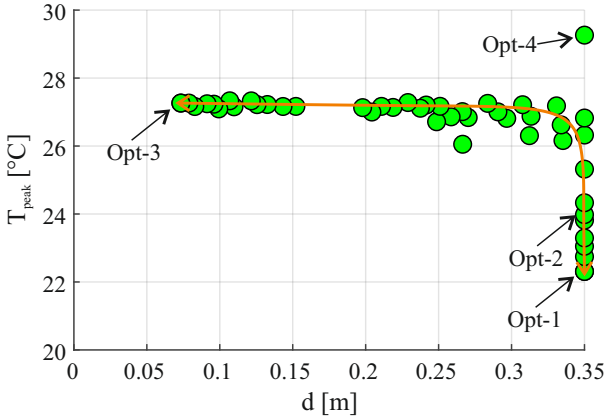


**Figure 6.** Relationship between optimal design variables for Case A.

### *3.2. Optimization of Case B*

Figure 7 shows the optimization results obtained for Case B. These include the Pareto front between heating and cooling loads, all the feasible designs evaluated during the optimization, and the baseline model. It can be seen that the limits of the bi-objective space have considerably changed compared to Case A because of incorporating the thermal conductivity in the design space. Here, the designs on the Pareto front achieve good load reductions for both heating and cooling.

To enable a quantitative analysis, Table 7 summarizes the performance of a few optimum designs obtained along with their relative improvements compared to the baseline model. Here, only the extreme optimal solutions for heating (Opt-1) and cooling (Opt-5) are discussed, since Opt-5 is also the best design for the total loads (heating + cooling).

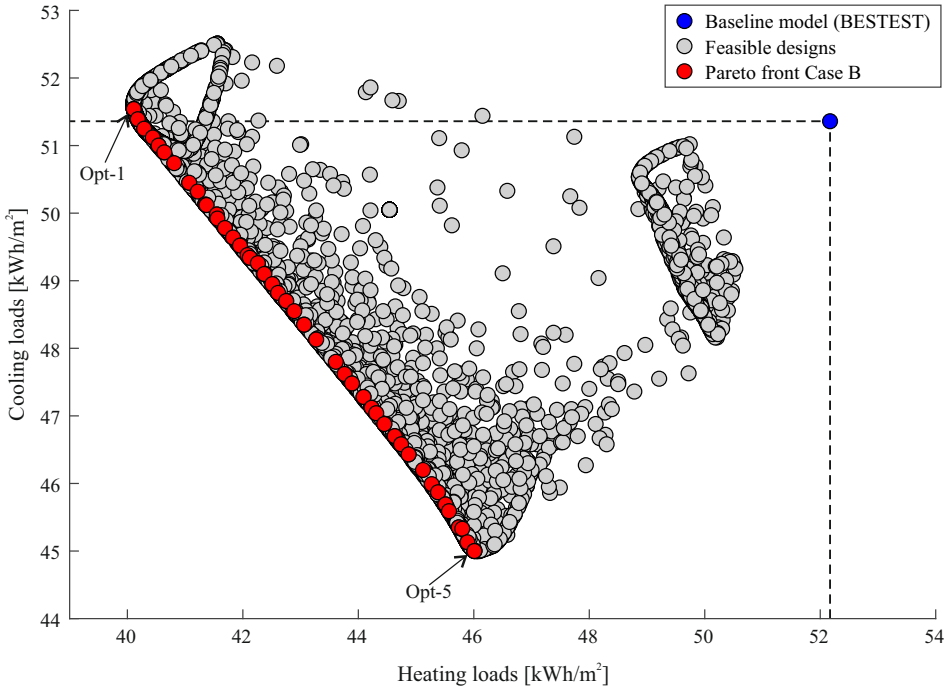


**Figure 7.** Optimization results of the annual ideal loads for heating and cooling obtained for Case B.

Opt-1 is the best design for heating, and the same is obtained in Case A. This is because the design space was only enlarged with higher thermal conductivity values than the original PCM-based panel. This aspect is more deeply analyzed in Section 3.3.

Opt-5 achieves load reductions of 11.81% and 12.38% for heating and cooling, respectively. Unlike the best design for cooling in Case A (Opt-3), Opt-5 achieves a large load reduction for cooling but also obtains a similar improvement for heating.

**Table 7.** Performances of the optimized designs for Case B. The best design for each case is in bold.

| | Heating Load (kWh/m$^2$) | Cooling Load (kWh/m$^2$) | Total Load (kWh/m$^2$) | Heating Saving (%) | Cooling Saving (%) | Total Saving (%) |
|---|---|---|---|---|---|---|
| Baseline | 52.17 | 51.36 | 103.53 | - | - | - |
| Opt-1 | 40.11 | 51.54 | 91.65 | **23.12** | −0.35 | 11.47 |
| Opt-5 | 46.01 | 45.00 | 91.01 | 11.81 | **12.38** | **12.09** |

Figure 8 shows the relationship between the design variables for all the optimum designs (Pareto front) of Case B. Due to all the optimal solutions having the thickest panel allowed (0.35 m), this graph only shows the relationship between the $T_{peak}$ and thermal conductivity of the panel (k). As previously introduced, the best building performance for heating (Opt-1) is achieved by using a $T_{peak}$ = 22.31 °C and the lowest thermal conductivity allowed of k = 0.473 W/(m·K). Conversely, the best building performance for cooling (Opt-5), which is also the best for the total loads, is achieved by using the highest thermal conductivity allowed of k = 10 W/(m·K) and a $T_{peak}$ = 26.24 °C. As a general guide, starting from the Opt-1 design to improve the cooling performance and going over the optimal designs, these employ a low thermal conductivity (<1 W/(m·K)) while increasing the $T_{peak}$ up to 25–26 °C. After that sector, the solutions that improve the cooling performance even more keep using a $T_{peak}$ = 25–26 °C while increasing their thermal conductivity.

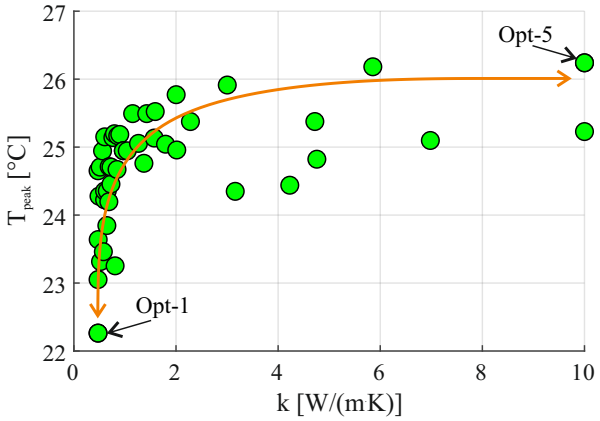


**Figure 8.** Relationship between optimal design variables for Case B.

### *3.3. Discussion*

Figure 9 shows the Pareto fronts obtained for both case studies (Case A and Case B) and the reference of the baseline model. As shown, the performance of the building for heating and cooling has a mutually contradictory response regarding the optimum design thermophysical properties of the PCM-based panels. This highlights the need of using the multiobjective approach herein proposed to design passive PCM-based systems in building applications. This novel approach presents several advantages compared to previous single optimization approaches found in the literature [9,26]; it allows for a better understanding of the real performance of passive PCM-based systems in buildings, such as those discussed next. In Figure 9, it can be also observed that the optimal solutions of Case B can considerably improve the building performance for cooling compared to either Case A or the reference building. This reveals that when the panel increases its thickness to incorporate more MPCM into the building, the panel must have a high thermal conductivity to guarantee the effectiveness of the extra MPCM incorporated. Therefore, beyond its optimum melting temperature, the PCM has to be thermally coupled with the indoor air to achieve the desired effect. Conversely, if the thickness of the panel increases but keeps a low thermal conductivity, part of the MPCM cannot provide its full storage/release capacity and does not affect the indoor air, which is the real target to reduce the loads. This aspect could be a limitation for standard microencapsulation technology embedded in cement-based pastes.

The volume fraction of the MPCM in cement pastes has a physical limit. Most studies available in the literature employ volume fractions of 20%, while only a few works considered higher amounts (up to a maximum of 40%) [56]. However, of this volume of MPCM, approximately 60% corresponds to the encapsulating shell, resulting in a very low effective fraction of PCM in the panel. This drives the need to use thicker panels to include more MPCM in the building, but as shown, increasing the thickness is not effective, because a part of the extra PCM added does not result in a thermal coupling with the indoor air and cannot drive a positive effect to it.

Finally, Figure 10 shows the monthly heating and cooling loads for the designs Opt-2 and Opt-5 compared to the baseline model. Regarding Opt-2, it reduces the heating loads for all the months with noticeable improvements in the autumn months. Conversely, this design has a similar performance to the baseline model regarding the cooling loads. It is worth remembering that the Opt-2 design (attained in the optimization of Case A) has more capacity to reduce the annual heating load (22.73%) than the cooling ones (0.25%).

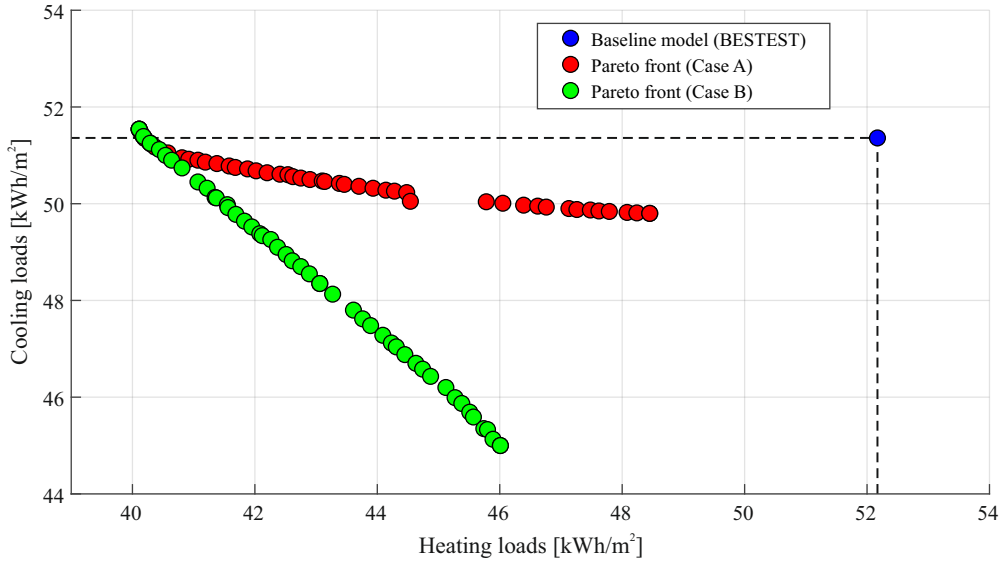


**Figure 9.** Comparison of the Pareto fronts for Case A and Case B.

Regarding Opt-5, the results also show a reduction in the heating loads for all months but with lower performance than the Opt-2 during the winter months. This design also reduces the cooling loads for all the months compared to the baseline model. However, the major cooling load improvements, reducing up to half of the loads, are achieved during moderate temperature months, such as the spring months. It may be worth remembering that this design (Opt-5), achieved in the optimization of Case B, has a good and balanced capacity to reduce the annual heating loads (11.81%) as well as the cooling ones (12.38%).

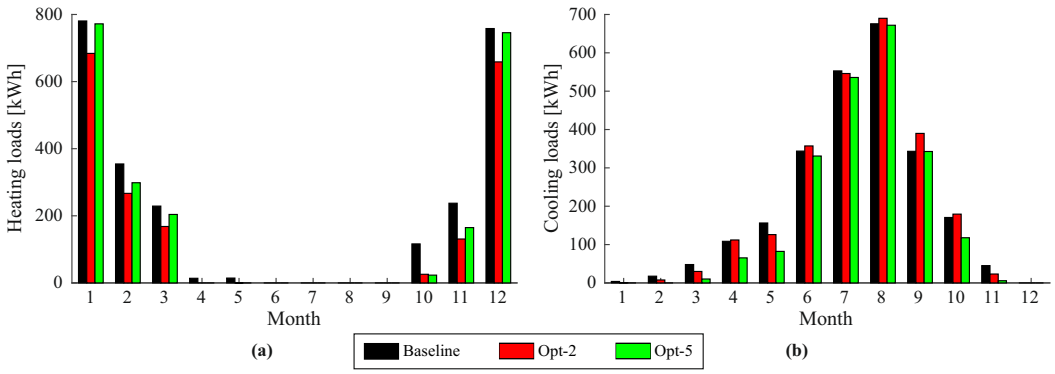


**Figure 10.** Monthly loads for the designs Opt-2 and Opt-5, and the baseline model. (**a**) Heating loads; (**b**) Cooling loads.

## 4. Conclusions

A multiobjective computational method to optimize the thermophysical properties of cementitious building panels enhanced with microencapsulated phase change materials (MPCMs) was developed. This comprises an automatic simulation-based optimization process that dynamically couples the NSGA-II optimizer with the EnergyPlus software. The BESTEST 900 in Sofia (Bulgaria-EU) was employed as a case study building to find the best trade-off between annual heating and cooling loads.

Based on the optimization results reported, the following concluding remarks can be drawn:

- In the first case study, named Case A, the PCM melting temperature and the thickness of the panel were considered as the design variables. Regarding the performance of the optimized panel enhanced with MPCM, there is a design that can reduce the heating loads up to 23% and another design that can reduce the cooling loads up to 3%.

To achieve this, a thick panel using a PCM melting temperature of 22 °C is preferred for minimizing the heating loads. Conversely, a thin panel employing a PCM melting temperature of 27 °C is required for minimizing the cooling loads.

- In Case B, the thermal conductivity of the panel was simultaneously optimized along with the with the design variables of Case A. The optimization results showed that the effectiveness of the PCM can be considerably improved if the thermal conductivity of the panel is increased. Compared to Case A, a 12.4% of cooling reduction is achieved by combining the maximum thermal conductivity with a PCM melting temperature of 26 °C. This highlights that the thermal conductivity of the panel is a key feature to be considered in the design stage. In particular, when the thickness of the panel increases to incorporate more MPCM into the building, some of these MPCMs are not thermally coupled with the indoor air, and this drives no positive effect in terms of cooling load reductions.
- Regarding the results discussed in the previous point, some limitations for the technology of cement-based panels enhanced with MPCM can be found in real applications. The low effective volume fraction of PCM because of the encapsulation technique, combined with the current structural limit for the MPCM volume in the cement pastes (normally 20%, and 30–40% in special cases), leads to the necessity of increasing the thickness of the panel to incorporate more PCM into the building. However, an increased thickness could affect the overall thermal conduction of the system, which is crucial for exploiting the PCM benefits.
- As a general conclusion, we can state the relevance of using whole building performance simulation tools to design PCM in buildings. For instance, a physically reasonable range of PCM melting temperatures (22–27 °C) was found by using EnergyPlus. Another important observation is the mutually contradictory nature of the heating and cooling loads regarding the thermophysical properties of the MPCM-based panel. This points out the need for using a multiobjective optimization approach to find the optimal designs.
- Finally, the major relative load reductions compared to the baseline model are achieved for the months with moderate temperatures (autumn/spring). This is because in these months, the effectiveness of the PCM-based panels improves thanks to an increment in the daily indoor temperature cycles.

Future works will be focusing on evaluating the optimum design of the PCM-based cementitious systems in more realistic multi-zone buildings and different typologies (residential/commercial).

**Author Contributions:** Conceptualization, F.B. and A.C.; methodology, F.B.; software, F.B.; formal analysis, F.B.; investigation, F.B.; resources, F.B.; data curation, F.B.; writing—original draft preparation, F.B.; writing—review and editing, F.B., A.C. and E.A.B.K.; supervision, F.B. and A.C.; visualization, F.B.; project administration, F.B. and E.A.B.K.; funding acquisition, F.B. and E.A.B.K. All authors have read and agreed to the published version of the manuscript.

**Funding:** The results found in this work are part of the 0E-BUILDINGS action. This project has received funding from the European Union's Horizon 2020 research and innovation programme under the Marie Skłodowska-Curie grant agreement N° 101024627. This work also represents a study of the research activities of the NRG-STORAGE project (grant agreement N° 870114, www.nrg-storage.eu, accessed on 1 June 2022, financed by the European Union H2020 407 Framework under the LC-EEB-01-2019 call, H2020-NMBP-ST-IND-2018-2020/H2020-NMBP-EEB-2019, IA type.

**Institutional Review Board Statement:** Not applicable.

**Informed Consent Statement:** Not applicable.

**Data Availability Statement:** For closer analysis (or their reproduction), the optimization results and the EnergyPlus models can be found at http://dx.doi.org/10.5281/zenodo.5675154, accessed on 20 June 2022.

**Acknowledgments:** We acknowledge support from the Deutsche Forschungsgemeinschaft (DFG, German Research Foundation) and the Open Access Publishing Fund of Technische Universität Darmstadt.

**Conflicts of Interest:** The authors declare no conflict of interest. The funders had no role in the design of the study; in the collection, analyses, or interpretation of data; in the writing of the manuscript; or in the decision to publish the results.

## References

1. IPCC. *An IPCC Special Report on the Impacts of Global Warming of 1.5 °C above Pre-Industrial Levels and Related Global Greenhouse Gas Emission Pathways*; IPCC: Geneva, Switzerland, 2019.
2. Ciancio, V.; Salata, F.; Falasca, S.; Curci, G.; Golasi, I.; de Wilde, P. Energy demands of buildings in the framework of climate change: An investigation across Europe. *Sustain. Cities Soc.* **2020**, *60*, 102213. [CrossRef]
3. De Gracia, A.; Cabeza, L.F. Phase change materials and thermal energy storage for buildings. *Energy Build.* **2015**, *103*, 414–419. [CrossRef]
4. Cabeza, L.F.; Castell, A.; Barreneche, C.D.; De Gracia, A.; Fernández, A. Materials used as PCM in thermal energy storage in buildings: A review. *Renew. Sustain. Energy Rev.* **2011**, *15*, 1675–1695. [CrossRef]
5. Cascone, Y.; Capozzoli, A.; Perino, M. Optimisation analysis of PCM-enhanced opaque building envelope components for the energy retrofitting of office buildings in Mediterranean climates. *Appl. Energy* **2018**, *211*, 929–953. [CrossRef]
6. Zhou, Y.; Zheng, S.; Liu, Z.; Wen, T.; Ding, Z.; Yan, J.; Zhang, G. Passive and active phase change materials integrated building energy systems with advanced machine-learning based climate-adaptive designs, intelligent operations, uncertainty-based analysis and optimisations: A state-of-the-art review. *Renew. Sustain. Energy Rev.* **2020**, *130*, 109889. [CrossRef]
7. Memon, S.A. Phase change materials integrated in building walls: A state of the art review. *Renew. Sustain. Energy Rev.* **2014**, *31*, 870–906. [CrossRef]
8. Cai, R.; Sun, Z.; Yu, H.; Meng, E.; Wang, J.; Dai, M. Review on optimization of phase change parameters in phase change material building envelopes. *J. Build. Eng.* **2021**, *35*, 101979. [CrossRef]
9. Saffari, M.; De Gracia, A.; Fernández, C.; Cabeza, L.F. Simulation-based optimization of PCM melting temperature to improve the energy performance in buildings. *Appl. Energy* **2017**, *202*, 420–434. [CrossRef]
10. Saffari, M.; de Gracia, A.; Ushak, S.; Cabeza, L.F. Passive cooling of buildings with phase change materials using whole-building energy simulation tools: A review. *Renew. Sustain. Energy Rev.* **2017**, *80*, 1239–1255. [CrossRef]
11. Bre, F.; e Silva Machado, R.M.; Lawrie, L.K.; Crawley, D.B.; Lamberts, R. Assessment of solar radiation data quality in typical meteorological years and its influence on the building performance simulation. *Energy Build.* **2021**, *250*, 111251. [CrossRef]
12. Cabeza, L.F.; Mehling, H.; Hiebler, S.; Ziegler, F. Heat transfer enhancement in water when used as PCM in thermal energy storage. *Appl. Therm. Eng.* **2002**, *22*, 1141–1151. [CrossRef]
13. Frusteri, F.; Leonardi, V.; Vasta, S.; Restuccia, G. Thermal conductivity measurement of a PCM based storage system containing carbon fibers. *Appl. Therm. Eng.* **2005**, *25*, 1623–1633. [CrossRef]
14. Jiang, Z.; Ouyang, T.; Yang, Y.; Chen, L.; Fan, X.; Chen, Y.; Li, W.; Fei, Y. Thermal conductivity enhancement of phase change materials with form-stable carbon bonded carbon fiber network. *Mater. Des.* **2018**, *143*, 177–184. [CrossRef]
15. Lei, J.; Tian, Y.; Zhou, D.; Ye, W.; Huang, Y.; Zhang, Y. Heat transfer enhancement in latent heat thermal energy storage using copper foams with varying porosity. *Sol. Energy* **2021**, *221*, 75–86. [CrossRef]
16. Zhong, Y.; Zhao, B.; Lin, J.; Zhang, F.; Wang, H.; Zhu, Z.; Dai, Z. Encapsulation of high-temperature inorganic phase change materials using graphite as heat transfer enhancer. *Renew. Energy* **2019**, *133*, 240–247. [CrossRef]
17. Srivatsa, P.; Baby, R.; Balaji, C. Numerical investigation of PCM based heat sinks with embedded metal foam/crossed plate fins. *Numer. Heat Transf. Part A Appl.* **2014**, *66*, 1131–1153. [CrossRef]
18. Sanker, S.B.; Baby, R. Phase change material based thermal management of lithium ion batteries: A review on thermal performance of various thermal conductivity enhancers. *J. Energy Storage* **2022**, *50*, 104606. [CrossRef]
19. Zhao, C.; Opolot, M.; Liu, M.; Bruno, F.; Mancin, S.; Flewell-Smith, R.; Hooman, K. Simulations of melting performance enhancement for a PCM embedded in metal periodic structures. *Int. J. Heat Mass Transf.* **2021**, *168*, 120853. [CrossRef]
20. Praveen, B.; Suresh, S.; Pethurajan, V. Heat transfer performance of graphene nano-platelets laden micro-encapsulated PCM with polymer shell for thermal energy storage based heat sink. *Appl. Therm. Eng.* **2019**, *156*, 237–249. [CrossRef]
21. Du, Y.; Zhou, T.; Zhao, C.; Ding, Y. Molecular dynamics simulation on thermal enhancement for carbon nano tubes (CNTs) based phase change materials (PCMs). *Int. J. Heat Mass Transf.* **2022**, *182*, 122017. [CrossRef]
22. Al-Saadi, S.N.; Zhai, Z.J. Modeling phase change materials embedded in building enclosure: A review. *Renew. Sustain. Energy Rev.* **2013**, *21*, 659–673. [CrossRef]
23. Heim, D.; Clarke, J.A. Numerical modelling and thermal simulation of PCM–gypsum composites with ESP-r. *Energy Build.* **2004**, *36*, 795–805. [CrossRef]
24. Pedersen, C.O. Advanced Zone Simulation in EnergyPlus: Incorporation of Variable Properties and Phase Change Material (PCM) Capability. In Proceedings of the Building Simulation 2007, Beijing, China, 3–6 September 2007; pp. 1341–1345.

25. Ascione, F.; De Masi, R.F.; de Rossi, F.; Ruggiero, S.; Vanoli, G.P. Optimization of building envelope design for nZEBs in Mediterranean climate: Performance analysis of residential case study. *Appl. Energy* **2016**, *183*, 938–957. [CrossRef]
26. Arıcı, M.; Bilgin, F.; Nižetić, S.; Karabay, H. PCM integrated to external building walls: An optimization study on maximum activation of latent heat. *Appl. Therm. Eng.* **2020**, *165*, 114560. [CrossRef]
27. Parameshwaran, R.; Naresh, R.; Ram, V.V.; Srinivas, P. Microencapsulated bio-based phase change material-micro concrete composite for thermal energy storage. *J. Build. Eng.* **2021**, *39*, 102247. [CrossRef]
28. Drissi, S.; Ling, T.C.; Mo, K.H.; Eddhahak, A. A review of microencapsulated and composite phase change materials: Alteration of strength and thermal properties of cement-based materials. *Renew. Sustain. Energy Rev.* **2019**, *110*, 467–484. [CrossRef]
29. Konuklu, Y.; Ostry, M.; Paksoy, H.O.; Charvat, P. Review on using microencapsulated phase change materials (PCM) in building applications. *Energy Build.* **2015**, *106*, 134–155. [CrossRef]
30. *ANSI/ASHRAE Standard 140-2011*; Standard Method of Test for the Evaluation of Building Energy Analysis Computer Programs. American Society of Heating, Refrigerating and Air Conditioning Engineers (ASHRAE): Atlanta, GA, USA, 2011.
31. Henninger, R.H.; Witte, M.J. *EnergyPlus Testing with Building Thermal Envelope and Fabric Load Tests from ANSI/ASHRAE Standard 140-2011*; U.S. Department of Energy: Pittsburgh, PA, USA, 2013.
32. Crawley, D.B.; Lawrie, L.K.; Winkelmann, F.C.; Buhl, W.F.; Huang, Y.J.; Pedersen, C.O.; Strand, R.K.; Liesen, R.J.; Fisher, D.E.; Witte, M.J.; et al. EnergyPlus: Creating a new-generation building energy simulation program. *Energy Build.* **2001**, *33*, 319–331. [CrossRef]
33. National Renewable Energy Laboratory (NREL); U.S. Department of Energy's (DOE) Building Technologies Office (BTO). EnergyPlus™ v9.5. 2021. Available online: https://github.com/NREL/EnergyPlus/releases/tag/v9.5.0 (accessed on 20 June 2022).
34. Integrated Porous Cementitious Nanocomposites in Non-Residential Building Envelopes for Green Active/Passive Energy STORAGE (NRG-STORAGE), Grant Agreement ID: 870114. Available online: https://cordis.europa.eu/project/id/870114 (accessed on 20 June 2022).
35. Crawley, D.B.; Shirey, D.; Cornick, S.; Jarrett, P.; Lott, J.; Morris, R.; Walker, I.; Walter, W.; Hall, R.; Anderson, J.; et al. ANSI/ASHRAE Standard 169-2013. Climatic data for building design standards. *ASHRAE Stand.* **2013**, *8400*, 786–798.
36. Peel, M.C.; Finlayson, B.L.; McMahon, T.A. Updated world map of the Köppen-Geiger climate classification. *Hydrol. Earth Syst. Sci.* **2007**, *11*, 1633–1644. [CrossRef]
37. Crawley, D.B.; Lawrie, L.K. 2020. Available online: https://climate.onebuilding.org/ (accessed on 1 October 2021).
38. Mankel, C.; Caggiano, A.; Ukrainczyk, N.; Koenders, E. Thermal energy storage characterization of cement-based systems containing microencapsulated-PCMs. *Constr. Build. Mater.* **2019**, *199*, 307–320. [CrossRef]
39. BASF. Datenblatt Micronal PCM DS 5038 X, (11/2013). Available online: https://thermalmaterials.org/pcm/micronal-ds-5038-x (accessed on 20 June 2022).
40. Tabares-Velasco, P.C.; Christensen, C.; Bianchi, M.; Booten, C. *Verification and Validation of EnergyPlus Conduction Finite Difference and Phase Change Material Models for Opaque Wall Assemblies*; Technical Report; National Renewable Energy Lab. (NREL): Golden, CO, USA, 2012.
41. Tabares-Velasco, P.C.; Christensen, C.; Bianchi, M. Verification and validation of EnergyPlus phase change material model for opaque wall assemblies. *Build. Environ.* **2012**, *54*, 186–196. [CrossRef]
42. U.S. Department of Energy. *Engineering Reference—EnergyPlus 9.5*; The Reference to EnergyPlus Calculation; U.S. Department of Energy: Washington, DC, USA, 2021.
43. Fachinotti, V.D.; Bre, F.; Mankel, C.; Koenders, E.A.; Caggiano, A. Optimization of multilayered walls for building envelopes including PCM-based composites. *Materials* **2020**, *13*, 2787. [CrossRef] [PubMed]
44. Mankel, C.; Caggiano, A.; König, A.; Said Schicchi, D.; Nazari Sam, M.; Koenders, E. Modelling the thermal energy storage of cementitious mortars made with PCM-recycled brick aggregates. *Materials* **2020**, *13*, 1064. [CrossRef] [PubMed]
45. Klimeš, L.; Charvát, P.; Joybari, M.M.; Zálešák, M.; Haghighat, F.; Panchabikesan, K.; El Mankibi, M.; Yuan, Y. Computer modelling and experimental investigation of phase change hysteresis of PCMs: The state-of-the-art review. *Appl. Energy* **2020**, *263*, 114572. [CrossRef]
46. Bre, F.; Peralta, I.; Caggiano, A.; Koenders, E. Impact of modeling the hysteresis phenomenon of phase change materials on the building performance simulation. In Proceedings of the BauSIM 2022—9th Conference of IBPSA Germany and Austria, Weimar, Germany, 20–22 September 2022.
47. Bre, F.; Roman, N.; Fachinotti, V.D. An efficient metamodel-based method to carry out multi-objective building performance optimizations. *Energy Build.* **2020**, *206*, 109576. [CrossRef]
48. Pareto, V. *Cours D'Economie Politique*; F. Rouge: Lausanne, Switzerland, 1896; Volume 1.
49. Deb, K.; Pratap, A.; Agarwal, S.; Meyarivan, T. A fast and elitist multiobjective genetic algorithm: NSGA-II. *IEEE Trans. Evol. Comput.* **2002**, *6*, 182–197. [CrossRef]
50. Hamdy, M.; Nguyen, A.T.; Hensen, J.L. A performance comparison of multi-objective optimization algorithms for solving nearly-zero-energy-building design problems. *Energy Build.* **2016**, *121*, 57–71. [CrossRef]
51. Zitzler, E.; Laumanns, M.; Thiele, L. *SPEA2: Improving the Strength Pareto Evolutionary Algorithm*; TIK-Report; Eidgenössische Technische Hochschule Zürich (ETH), Institut für Technische Informatik und Kommunikationsnetze (TIK): Zürich, Switzerland, 2001; Volume 103.

52. Eberhart, R.; Kennedy, J. A new optimizer using particle swarm theory. In Proceedings of the Sixth International Symposium on Micro Machine and Human Science, MHS'95, Nagoya, Japan, 4–6 October 1995; pp. 39–43.
53. Kheiri, F. A review on optimization methods applied in energy-efficient building geometry and envelope design. *Renew. Sustain. Energy Rev.* **2018**, *92*, 897–920. [CrossRef]
54. Bre, F.; Fachinotti, V.D. A computational multi-objective optimization method to improve energy efficiency and thermal comfort in dwellings. *Energy Build.* **2017**, *154*, 283–294. [CrossRef]
55. Fortin, F.A.; De Rainville, F.M.; Gardner, M.A.G.; Parizeau, M.; Gagné, C. DEAP: Evolutionary algorithms made easy. *J. Mach. Learn. Res.* **2012**, *13*, 2171–2175.
56. Sam, M.; Caggiano, A.; Dubyey, L.; Dauvergne, J.L.; Koenders, E. Thermo-physical and Mechanical Investigation of Cementitious Composites enhanced with Microencapsulated Phase Change Materials for Thermal Energy Storage. *Constr. Build. Mater.* **2022**, *340*, 127585. [CrossRef]